Symmetry energy and experimentally observed cold fragments in intermediate heavy-ion collisions *

Su-Ya-La-Tu Zhang(张苏雅拉吐)[1] Mei-Rong Huang(黄美容)[1;1)] R. Wada[2;2)] Xing-Quan Liu(刘星泉)[3]
Wei-Ping Lin(林炜平)[3] Jian-Song Wang(王建松)[3]

[1]College of Physics and Electronics Information, Inner Mongolia University for Nationalities, Tongliao 028000, China
[2]Cyclotron Institute, Texas A&M University, College Station, TX 77843, USA
[3]Institute of Modern Physics, Chinese Academy of Sciences, Lanzhou 730000,China

Abstract: An attempt is made to study the symmetry energy at the time of primary fragment formation from the experimentally observed cold fragments for a neutron-rich system of ^{64}Ni + ^{9}Be at 140 MeV/nucleon, utilizing the recent finding that the excitation energy becomes lower for more neutron-rich isotopes with a given Z value. The extracted $a_{\rm sym}/T$ values from the cold fragments, based on the Modified Fisher Model (MFM), are compared to those from the primary fragments of the antisymmetrized molecular dynamics (AMD) simulation and become consistent with the simulation when the $I = N - Z$ value becomes larger, indicating that the excitation energy of these neutron-rich isotopes is indeed lower.

Keywords: symmetry energy, modified Fisher model, antisymmetrized molecular dynamics simulations

PACS: 25.70.Pq **DOI:** 10.1088/1674-1137/41/4/044001

1 Introduction

The symmetry energy term in the nuclear equation of state (EOS) is intimately related to the dynamical processes of nuclear reactions, the characteristic structure of nuclei and astrophysical phenomena [1, 2]. In our recent works [3–7], we used isotopic yields to investigate the symmetry energy, based on the Modified Fisher Model (MFM) [8–12]. With this model, the symmetry energy values relative to the temperature, $a_{\rm sym}/T$, were extracted from the experimentally observed cold fragments [3, 4, 13], the reconstructed primary hot isotopes [5, 6] and simulated primary isotopes from a transport model [7]. The isobaric yield method has been also applied to the experimental and theoretical studies of projectile-like fragment production [14–17]. In these studies, it is found that the secondary cooling process, after the formation of the primary hot isotopes, changes the isotope distributions drastically and a significant mass dependence of the extracted $a_{\rm sym}/T$ values is observed for the experimentally observed cold isotopes, whereas the $a_{\rm sym}/T$ values from the yields of the reconstructed hot isotopes and the primary hot isotopes show a much smaller mass dependent distribution. In a recent theoretical study by Mallik et al. [17], they also pointed out that serious errors may occur when one tries to study the symmetry energy and temperature at the time of fragment formation from the cold isotope yields.

In one of our previous studies, the primary hot fragments were experimentally reconstructed [18] with a kinematical focusing technique. However, in order to do that, neutrons have to be measured besides the charged particles in coincidence with isotopically resolved fragments, since neutron emissions are dominant in the secondary cooling process. This is a difficult task, especially in a 4π detection system. In this article, an alternative method is presented, utilizing the very neutron-rich cold isotopes. In Ref. [18], the excitation energy of the primary hot isotopes was reconstructed and it was found that the excitation energy decreases when the $I = N - Z$ becomes large among isotopes with a given Z, as shown in Fig. 1. This observation suggests that the sequential decay effect on the isotope distributions becomes small for such neutron-rich isotopes. In Ref. [15], Ma et al. extracted $a_{\rm sym}/T$ of symmetric and neutron-rich fragments from the experimental cold isotope distributions of Mocko et al. [19] by three different approximation methods using the isobaric yield ratios (IYRs), in which the effects from different excitation energies and sequential

Received 4 September 2016

∗ Supported by National Natural Science Foundation of China (U1432247, 11605097), National Basic Research Program of China (973 Program, 2014CB845405), Doctoral Scientific Research Foundation of Inner Mongolia University for the Nationalities (BS365)

1) E-mail: huangmeirong@imun.edu.cn

2) E-mail: wada@comp.tamu.edu

decays can be investigated. They also reported that the mass dependence of the $a_{\rm sym}/T$ values becomes smaller when the I value of the isotopes increases. The $a_{\rm sym}/T$ values also become smaller when larger isobars are used as the reference in the IYR method. In this article we pursue this finding further and look for the possibility of determining the symmetry energy at the time of fragment formation from cold neutron-rich isotopes, using the experimental isotope yields from ^{64}Ni + ^{9}Be at 140 MeV/nucleon from one of the experiments performed by Mocko et al. at the National Superconducting Cyclotron Laboratory (NSCL) at Michigan State University (MSU) [19]. The ^{64}Ni + ^{9}Be reaction is chosen to get more neutron-rich cold isotopes in the experiment.

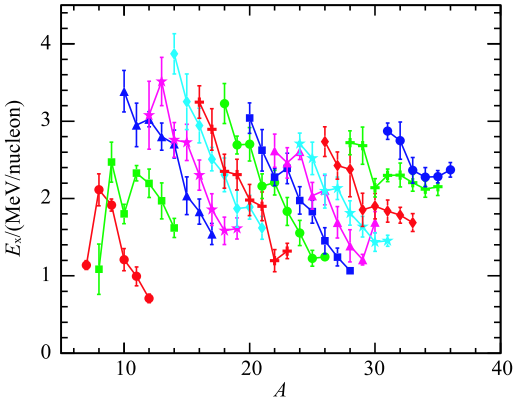

Fig. 1. (color online) Excitation energy of the reconstructed primary isotopes as a function of isotope mass A for different elements with $Z=4$ (red dots) to $Z=16$ (blue dots). The results of the isotopes with a given Z are connected by lines to guide the eye. The maximum of I values for the majority of isotopes is $I=6$ in this data set. The data are taken from Ref. [18].

2 Extraction of $a_{\rm sym}/T$ from experimentally observed cold fragments

In the framework of MFM [10–12, 20], the yield of an isotope with $I=N-Z$ and A (N neutrons and Z protons), produced in a multi-fragmentation process, can be given as

$$Y(I,A)=Y_0\cdot A^{-\tau}\exp\Big[\frac{W(I,A)+\mu_{\rm n}N+\mu_{\rm p}Z}{T}+S_{\rm mix}(I,A)\Big]. \quad (1)$$

Using the generalized Weizsäcker-Bethe semiclassical mass formula [21, 22], $W(I,A)$ can be approximated as

$$W(I,A)=a_{\rm v}A-a_{\rm s}A^{2/3}-a_{\rm c}\frac{Z(Z-1)}{A^{1/3}}-a_{\rm sym}\frac{I^2}{A}-a_{\rm p}\frac{\delta}{A^{1/2}},\quad \delta=-\frac{(-1)^Z+(-1)^N}{2}. \quad (2)$$

In Eq. (1), $A^{-\tau}$ and $S_{\rm mix}(I,A)=-N\ln(N/A)-Z\ln(Z/A)$[1)] originate from the increases in the entropy and the mixing entropy, respectively, at the time of fragment formation. $\mu_{\rm n}$ ($\mu_{\rm p}$) is the neutron (proton) chemical potential. τ is the critical exponent. In this work, the value of $\tau=2.3$ is adopted from the previous studies [20]. In general, the coefficients $a_{\rm v}$, $a_{\rm s}$, $a_{\rm sym}$, $a_{\rm p}$ and the chemical potentials are temperature and density dependent, even though these dependencies are not shown explicitly in Eq. (2).

To further investigate the secondary effects on extraction of the symmetry energy coefficient, these two equations are used, as Ref. [15] obtained:

$$\frac{a_{\rm sym}}{T}=\frac{A}{4(I+1)}\{[\Delta\mu+2a_{\rm c}(Z-1)/A^{1/3}]/T-\ln[R(I+2,I,A)]+\Delta_I\}, \quad (3)$$

$$\frac{a_{\rm sym}}{T}=\frac{A}{8}\{[\ln[R(I,I-2,A)]-\ln[R(I+2,I,A)]-\Delta_{I-2}+\Delta_I-2a_{\rm c}/(A^{1/3}T)\}. \quad (4)$$

In both expressions, the pairing terms are omitted, because only odd-I isotopes are taken into account in the following analysis in this section. $R(I_2,I_1,A)=Y(I_2,A)/Y(I_1,A)$ and $Y(I,A)$ is the yield of isotope with mass number A and I. $\Delta_I=S_{\rm mix}(I+2,A)-S_{\rm mix}(I,A)$. $\Delta\mu=\mu_{\rm n}-\mu_{\rm p}$. In our previous works [3, 5, 6], $\Delta\mu/T$ and $a_{\rm c}/T$ values were determined, using mirror isobars ratio of $I=1$ and -1, employing the following relation [3].

$$\ln[R(1,-1,A)]=[\Delta\mu+2a_{\rm c}(Z-1)/A^{1/3}]/T. \quad (5)$$

However in the data set of Mocko et al. for ^{64}Ni+^{9}Be [19], very few isotopes with $I=-1$ are available. Therefore the $\Delta\mu/T$ and $a_{\rm c}/T$ values are taken from Ref. [15], in which these values were determined by a global parameter fit, as $\Delta\mu/T=-1.27$ and $a_{\rm c}/T=0.64$.

In Fig. 2, the results from Eq. (3) are plotted as a function of isotope mass A for $I=3$, 5, and 7, together with the AMD results. The mass dependence of the $a_{\rm sym}/T$ values for the experimental data becomes small as I becomes large. In Refs. [3, 4], we pointed out that the mass dependence originates from the secondary cooling process of the primary hot isotopes and we expect that the effect becomes smaller when the excitation energy becomes lower. Therefore we interpret

1) Eq.(1) has the opposite sign for the mixing entropy, compared to the formulation in Refs. [11, 12]. We believe that they are wrong. We have been using their formula for all our previous publications and we are writing errata for them. The methodology and the global trend of the extracted values are the same, but the extracted values such as density, temperature and symmetry energy change by about 10%-20%. See details in the forthcoming errata.

the decreasing mass dependence as I increases for the experimental data in the figure as the reflection of the lower excitation energy of isotopes as I increases, shown in Fig. 1. In order to get the $a_{\rm sym}/T$ values without the secondary cooling effect, the AMD transport model of Ono et al. [23–25] is employed with the standard Gogny interaction. The clusters are produced naturally in AMD calculations, and early recognition of clusters relies on a physical space coalescence radius parameter. The values of $R_{\rm c}=5$ fm and evolution time = 300 fm/c were adopted from Refs. [3], and can reproduce the experimental data better than $R_{\rm c}=1.5$ fm and evolution time = 150 fm/c. Previous studies have shown there is a "statistical" behavior for the multiplicity of primary fragments IMF [26] even if there is no equilibrium in the AMD simulations, thus, directly using Eq. (3) for primary fragments obtained in AMD can help us to understand the sequential decay effects on the extraction of $a_{\rm sym}/T$ by comparing the results between AMD primary fragments and experiment cold fragments. Since the experiment was performed in a reverse kinematics, all generated IMFs are assumed as "experimentally detected" in the analysis and no filter for the experimental conditions is employed. The AMD results are obtained from Eq. (3) as the average values over all odd I values and are shown by blue triangles in Fig. 2. It shows a rather flat distribution as a function of A. There is still a large gap between the results of $I=7$ and those of the AMD primary hot isotopes, indicating that the sequential decay contribution remains in the most neutron-rich isotopes observed in the experiment, even though the effect becomes smaller for the larger I values.

The AMD simulation does not predict the lower excitation energy of neutron-rich isotopes and predicts more or less constant excitation energies among different isotopes for a given Z value, as discussed in Ref. [18]. However the experimentally reconstructed hot isotope distributions are well reproduced by the simulation [5, 6]. Up to now we do not know the mechanism of the isotope dependence of the excitation energy in the simulation, but we use the $a_{\rm sym}/T$ value from the AMD primary hot isotope yields as a standard for the values at the time of the fragment formation in this work.

In order to see the sequential decay effects in Eq. (3) in more detail, the right-hand side of Eq. (3) is divided into three terms and plotted separately in Fig. 3(a) for the case of $I=7$. The summed spectrum, $Y=Y_1-Y_2+Y_3$, is shown in Fig. 3(c). One can easily see that the significant increase seen in Fig. 3(c) is from the term $Y_1=\frac{A}{32}[\Delta\mu+2a_{\rm c}(Z-1)/A^{1/3}]/T$ in Fig. 3(a). As shown in Eq. 5, these terms are closely related to the isotope yields of $I=-1$ and 1, where the isotopes are at a higher excitation energy according to Fig. 1. Therefore the sequential decay effect becomes large in Y_1.

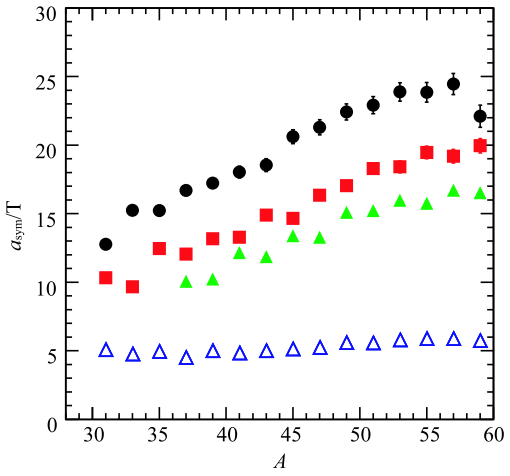

Fig. 2. (color online) Extracted $a_{\rm sym}/T$ values from Eq. (3) for $I=3$ (dots), 5 (squares) and 7 (closed triangles). The results of the AMD simulation is also shown by open triangles, which is the values averaged over those of $I=3,5$ and 7.

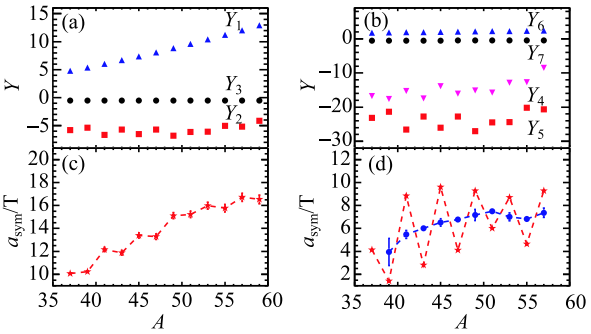

Fig. 3. (color online) (a)Values of the different terms in Eq. (3) as a function of A for the case of $I=7$. Triangles are for $Y_1=\frac{A}{32}[\Delta\mu+2a_{\rm c}(Z-1)/A^{1/3}]/T$. Squares are for $Y_2=\frac{A}{32}\ln[R(9,7,A)]$. Dots are for $Y_3=\frac{A}{32}\Delta_7$. (b) Same as (a), but using Eq. (4). Inverted triangles are for $Y_4=\frac{A}{8}\ln[R(7,5,A)]$. Squares are for $Y_5=\frac{A}{8}\ln[R(9,7,A)]$. Triangles are for $Y_6=\frac{A}{4}a_{\rm c}/(A^{1/3}T)$. Dots are for $Y_7=\frac{A}{8}(\Delta_7-\Delta_5)$. (c) $a_{\rm sym}/T=Y_1-Y_2+Y_3$ values from (a) (Eq. (3)) versus A. (d) $a_{\rm sym}/T=Y_4-Y_5-Y_6+Y_7$ values from (b) (Eq. (4)) versus A shown by stars. Dots represent the values averaged over the neighboring points.

In order to minimize the sequential decay effect, Eq. (4) is examined, which relates only isotopes with larger I values. Here the $a_{\rm sym}/T$ value is expressed as the difference of two isobar ratios, $\ln[R(I,I-2,A)]$ and $\ln[R(I+2,I,A)]$. The right-hand side of Eq. (4) is divided

into four terms Y_4, Y_5, Y_6, Y_7, and the definition of each term and the values are shown for $I=7$ in Fig. 3(b). The summed Y values are plotted by stars in Fig. 3(d). As one can see in Fig. 3(b), the contribution from Coulomb term Y_6 and that from the mixing entropy term Y_7 are small, compared to the other two terms. Therefore in Eq. (4) the $a_{\rm sym}/T$ values are determined essentially from the three isobars with $I=5,7$ and 9, which have rather low excitation energies according to Fig. 1, and therefore smaller mass dependence is expected. However, as seen in the figure, the Y_4 and Y_5 terms show staggering and their phases are opposite. These staggerings were attributed to the even-odd shell effect in the sequential decay cascade process in one of our previous studies [3]. These staggering were also observed in other experiments and similar explanations were presented [27, 28]. For very neutron-rich isotopes, the neutron separation energy becomes small and dominates the particle decay from an excited nucleus when the excitation energy becomes low. The isotopes with a lower neutron threshold tend to make a neutron decay easier and end up with less yield at the ground state. The observed staggering is, therefore, governed by the neutron separation energy between isotopes with the same mass in $R(I+2,I,A)$ for isotopes with a large I value. As an example, for the case of $I=7$, the correlation of $\ln[R(9,7,A)]$ and neutron separation energy, Sn, of isotopes with $I=9$ and 7 are shown in Fig. 4(a) and (b), respectively. Sn values oscillate when A changes every two units and the patterns are opposite between isotopes with $I=9$ and those with $I=7$. For $A=37$, for example, the shell effect causes Sn to be lower for $I=9$ and higher for $I=7$, resulting in smaller yields for $I=9$ and larger for $I=7$. This results in the smaller value of $\ln[R(9,7,37)]$ relative to that without the shell effect. The opposite situation occurs for $A=39$, making $\ln[R(9,7,39)]$ larger. This pattern is repeated and causes the staggering observed in Fig. 3(b). The same thing happens for the case of $I=5$, but they oscillate in opposite phase. Since the $a_{\rm sym}/T$ values are given by the difference between $\ln[R(I+2,I,A)]$ with $I=7$ and $I=5$ in opposite phase, the staggering from Eq. (4) is enhanced as seen in Fig. 3(d), compared to that in Fig. 3(b) and (c). In (c) the staggering is reduced by a factor of 4 for the $I=7$ case, because of the pre-factor $\dfrac{A}{4(I+1)}$. The above discussions indicate that there is a weaker sequential decay effect on Eq. (4) than on Eq. (3), since Eq. (4) has many neutron-rich isotopes involved. Therefore, we will use Eq. (4) in the following analysis of values of $a_{\rm sym}/T$ from experiment data and simulations.

In order to evaluate the $a_{\rm sym}/T$ values without the shell effect, we assume the shell contribution to the value Y_4 or Y_5 in Eq. (4) as ΔY, a constant relative to the nearby points as an approximation. Then for a given A number, Y_4 and Y_5 can be expressed as $Y_4=Y_4^0\pm\Delta Y$ and $Y_5=Y_5^0\mp\Delta Y$, and thus $a_{\rm sym}/T=Y_4^0-Y_5^0\pm2\Delta Y$, where Y_4^0 and Y_5^0 are the values without the shell effect. The sign changes when A changes by two units and causes the observed staggering. Therefore, when we average over the results with neighboring points, ΔY contributions are canceled out and one can get approximate $a_{\rm sym}/T$ values without the staggering effect. The results are shown by dots in Fig. 3(d), which show a rather smooth trend as expected. The errors shown for the averaged values in Fig. 3(d) are evaluated as follows. As shown in Fig. 3(b) and (d), the shell correction is the major cause for the errors. In the above calculation of $a_{\rm sym}/T$, the shell corrections are taken into account as the average of neighboring three points. However the shell effect between $A-2$ and A and between A and $A+2$ are not symmetric in some cases. In order to evaluate the maximum and minimum of the corrections for $a_{\rm sym}/T(A)$, the average is made either between $a_{\rm sym}/T(A)$ and $a_{\rm sym}/T(A-2)$ or between $a_{\rm sym}/T(A-2)$ and $a_{\rm sym}/T(A+2)$. The errors attached in Fig. 3(d) correspond to the minimum and maximum of these shell corrections.

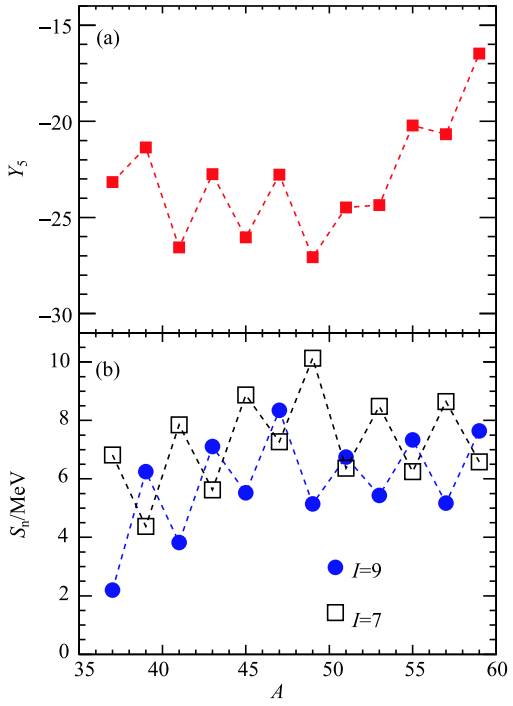

Fig. 4. (color online) (a) $Y_5=\ln[R(9,7,A)]$ as a function of A. (b) Neutron separation energy of $I=9$ (dots) and $I=7$ (squares) for isotopes with mass $A=37$ to 59. Data points are connected by lines to guide the eye.

In Fig. 5, the averaged $a_{\rm sym}/T$ values from Eq. (4) for $I=3,5$ and 7 are plotted from the experimental isotope yields, together with the results from the same equation for the AMD primary hot isotopes. The AMD results

are averaged over the corresponding I values, but not between the neighboring A values, since the AMD results are from the primary hot isotopes and do not show a notable staggering. The AMD results are very similar to those from Eq. (3) in Fig. 2 for $A > 35$. This is consistent with our assumptions that the significant mass dependence of the $a_{\rm sym}/T$ values originates from the sequential cooling process. Therefore the results from Eq. (3) and Eq. (4) should become similar for the AMD primary isotopes. The experimental $a_{\rm sym}/T$ values from Eq. (4) for $I = 3$ show a similar trend and values to those from Eq. (3) in Fig. 2, indicating a large contribution from the sequential cooling process. When the I value becomes larger, the mass dependence of the experimental $a_{\rm sym}/T$ values becomes small and for $I = 7$ (closed squares), the distribution shows a small mass dependent distribution and becomes almost identical to that of the AMD primary isotopes (triangles). However, these values are from the averaged values over the neighboring A and also depend slightly on the Coulomb parameter values, even though that contribution is small, as seen in Fig. 3(b). When we use the parameters from the AMD primary isotope distributions of $I = -1$ and 1, using Eq. (5), one gets $\Delta\mu/T = 0.5$ and $a_{\rm c}/T = 0.19$. Using these parameters, the resultant $a_{\rm sym}/T$ values for the case of $I = 7$ are shown by open circles in the bottom of Fig. 5. One can see about 1 MeV difference from those from the parameter values from Ref. [15]. Therefore, this ~ 1 MeV ambiguity in the extraction of $a_{\rm sym}/T$ values make it difficult to perform more detailed comparisons between the experimental distributions and those of the simulations, which is performed in Refs. [5–7]. To double check the sequential decay effect of the symmetry energy coefficients $a_{\rm sym}/T$ extracted by the isobaric yield ratio method, the excitation of AMD primary fragments was followed using the GEMINI code [29]. Fitting parameters $\Delta\mu/T = -0.65$ and $a_{\rm c}/T = 0.47$ were obtained by using the Eq. (5). The AMD+GEMINI results averaging over neighboring points for each I value are shown in Fig. 5 (stars). The decreasing of $a_{\rm sym}/T$ of fragments as I increases is consistent with the experimental results. It indicates that the sequential decay effect modifies the fragment distributions a lot when I is small, while it becomes weaker for very neutron-rich isotopes.

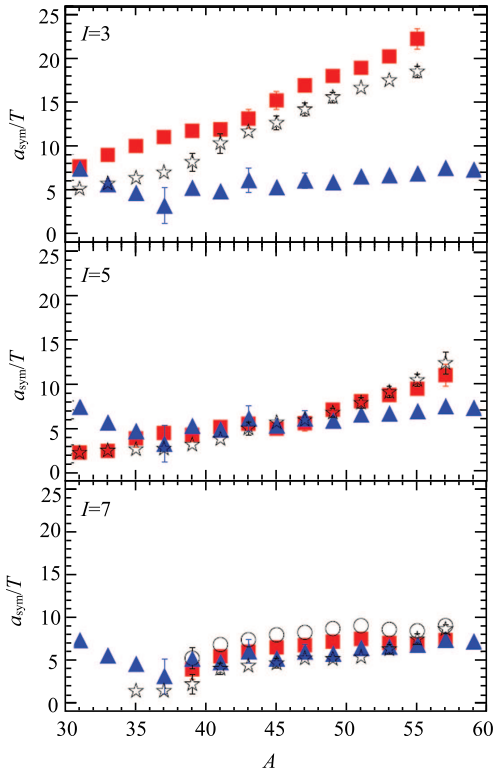

Fig. 5. (color online) $a_{\rm sym}/T$ from the experimental data (squares), the AMD simulations (triangles) and the AMD+GEMINI simulations (stars) versus A, using Eq. (4). The experimental and the AMD+GEMINI results are obtained by averaging over neighboring points for each I value. The I value is indicated in each figure. For $I = 7$, open circles indicate the experimental results from Eq. (4), but $\Delta\mu/T$ and $a_{\rm c}/T$ parameters from the AMD primary isotopes of $I = -1$ and 1. The AMD results are obtained by averaging over the corresponding values of $I = 3, 5$ and 7, but not averaging over neighboring points. The AMD results are the same in the three plots.

3 Conclusions

In summary, the $a_{\rm sym}/T$ values are extracted, using the isobaric yield ratio method, from the experimental cold isotope yields from ^{64}Ni+^{9}Be at 140 MeV/nucleon of Mocko et al. [19]. When neutron rich isotopes are used, the secondary sequential decay effect becomes small, consistent with our previous finding of the lower excitation energy for neutron-rich isotopes for a given Z value in Ref. [18]. Especially when Eq. (4) is utilized for $I = 7$, the averaged values of the extracted $a_{\rm sym}/T$ values around neighboring A values show a small mass-dependent distribution as a function of A and become very similar to those from the AMD primary isotopes, indicating that the secondary cooling effect is almost eliminated. Some ambiguities remain, however, which prevent more detailed analyses to study the density, symmetry energy and temperature as performed in our previous works.

We would like to acknowledge the HIRFL supercomputing center. One of the authors (R.W.) thanks the Senior International Scientists Visiting Professorship Program of the Chinese Academy of Sciences (2012T1JY3-2010T2J22) for their support.

References

1 Bao-An. Li et al, Phys. Rep., **464**: 113 (2008)
2 J. M. Lattimer and M. Prakash, Science, **23**: 536 (2004)
3 M. Huang et al, Phys. Rev. C, **81**: 044620 (2010)
4 M. Huang et al, Phys. Rev. C, **82**: 054602 (2010)
5 W. Lin et al, Phys. Rev. C, **89**: 021601(R) (2014)
6 W. Lin et al, Phys. Rev. C, **90**: 044603 (2014)
7 X. Liu et al, Phys. Rev. C, **90**: 014605 (2014)
8 A. Bonasera, F. Gulminelli, and J. Molitoris, Phys. Rep., **243**: 1 (1994)
9 A. Bonasera et al, Riv. Nuovo Cimento, **23**: 1 (2000)
10 M. E. Fisher, Rep. Prog. Phys., **30**: 615 (1967)
11 R. W. Minich et al, Phys. Lett. B, **118**: 458 (1982)
12 A. S. Hirsch et al, Nucl. Phys. A, **418**: 267c (1984)
13 Z. Chen et al, Phys. Rev. C, **81**: 064613 (2010)
14 C. W. Ma, F. Wang, Y. G. Ma and C. Jin, Phys. Rev. C, **83**: 064620 (2011)
15 C. W. Ma, J. Pu, S. S. Wang, H. L. Wei, Chin. Phys. Lett., **29**: 062101 (2012)
16 C. W. Ma, X. L. Zhao, J. Pu, S. S Wang, C.Y. Qiao, X. Feng, R. Wada, and Y. G. Ma, Phys. Rev. C, **88**: 014609 (2013)
17 S. Mallik and G. Chaudhuri, Phys. Rev. C, **87**: 011602R (2013)
18 M. R. D. Rodrigues et al, Phys. Rev. C, **88**: 034605 (2013)
19 M. Mocko et al, Phys. Rev. C, **74**: 054612 (2006)
20 A. Bonasera et al, Phys. Rev. Lett., **101**: 122702 (2008)
21 C. F. von Weizsäcker, Z. Phys., **96**: 431 (1935)
22 H. A. Bethe, Rev. mod. Phys., **8**: 82 (1936)
23 A. Ono and H. Horiuchi, Phys. Rev. C, **53**: 2958 (1996)
24 A. Ono, Phys. Rev. C, **59**: 853 (1999)
25 A. Ono, S. Hudan, A. Chbihi, J. D. Frankland, Phys. Rev. C, **66**: 014603 (2002)
26 X. Liu et al, Phys. Rev. C, **92**: 014623 (2015)
27 M. V. Ricciardi et al, Nucl. Phys. A, **733**: 299 (2004)
28 M. D. Agostino et al, Nucl. Phys. A, **861**: 47 (2011)
29 R. J. Charity et al, Nucl. Phys. A, **483**: 371 (1988)